RSC Advances

PAPER

View Article Online
View Journal | View Issue

Cite this: *RSC Adv.*, 2014, **4**, 56926

Poly(3,4-ethylenedioxythiophene)/MoS_2 nanocomposites with enhanced electrochemical capacitance performance

Jin Wang,*[a] Zongchao Wu,[a] Huabing Yin,[b] Wei Li[a] and Yang Jiang[c]

Composites based on conducting polymers and two-dimensional (2D) layer structure transition metal oxides are expected to realize the combination of good mechanical properties and excellent capacitance. Here poly(3,4-ethylenedioxythiophene)/molybdenum disulfide (PEDOT/MoS_2) intercalated composites were successfully synthesized *via in situ* polymerization in the presence of ammonium persulfate (APS). The thermal stability, conductivity and capacitance performance are improved significantly with increasing fraction of MoS_2. When the content of MoS_2 was 45% in weight, the maximum weight loss velocity temperature is 365 °C which is 52 °C higher than that of PEDOT; the specific capacitance was 405 F g^{-1}, about 4 times that of a PEDOT electrode; also the capacity retention was around 90% after 1000 cycles. This study provides a facile preparation method of organic/inorganic nanocomposites with enhanced electrochemical capacitance performance.

Received 19th October 2014
Accepted 27th October 2014

DOI: 10.1039/c4ra12683a

www.rsc.org/advances

1 Introduction

Supercapacitors possess outstanding properties such as the high power density typical of conventional capacitors together with the high energy density typical of rechargeable batteries. In addition, supercapacitors also exhibit fast charge–discharge processes and a long cycle life. These advantages mean they are expected to become an efficient and practical energy storage device.[1] Research into supercapacitors is largely focused on improving performance, reducing cost and improving the environmental friendliness of the devices. The most commonly used electrode materials include carbon material,[2] transition metal oxides[3,4] and conductive polymers.[5–8] There are limitations to a single species used for electrodes active materials, like carbon nanotubes, graphene and its derivatives typically have lower specific capacitances than conductive polymers, ruthenium dioxide (RuO_2) can suffer from poisoning, and conductive polymers usually possess poor cycle stability. These factors limit their application as electrode materials in supercapacitors.[9,10] Composites of conductive polymers and inorganic materials offer a promising combination of cycle stability, cost-efficiency and good capacitance performance.[11,12]

Supercapacitors work based on two charge-storage mechanisms: surface ion adsorption (electric double layer capacitance) and redox reactions (pseudocapacitance).[13] Conducting polymers are so-called pseudocapacitors, *i.e.*, they store charge, not only in the electrical double layer, but also faradaically in the polymer matrix.[14] Among these conductive polymers, poly(3,4-ethylenedioxythiophene) (PEDOT) possess the potential to be used as an electrode due to its superior conductivity and stability.[15] Additionally, PEDOT has a larger electrochemical window compared to other conducting polymers. It has been reported that PEDOT can be composited with transition metal oxide, graphene and carbon materials to prepare electrode materials.[16–18] Two-dimensional (2D) layered compounds such as graphite and transition metal oxides can offer a large surface area to storage charge, resulting in good characteristics for electric double layer capacitance.[19,20] Molybdenum disulfide (MoS_2) is a typical 2D layered material that is non-toxic, available at low cost and has been confirmed to have high specific capacity and cycle stability when used as an anode material.[21] The layered MoS_2 can be anticipated to exhibit good capacitive properties due to its sheetlike morphology, which provides a large surface area for double-layer charge storage. In addition, the transition metal Mo center can exhibit a range of oxidation states from +2 to +6, providing it pseudocapacitance abilities similar to RuO_2. Composites based on PEDOT and 2D layered MoS_2 are expected to offer the synergetic combination of good mechanical properties and excellent capacitance derived from both charge-storage mechanisms.

Conjugated polymer/MoS_2 composites can be prepared by means of the exfoliating/restacking technique of Li_xMoS_2. First, MoS_2 was intercalated by lithium to form Li_xMoS_2 and exfoliated into the single-molecule-layer MoS_2 suspension in water, and then in the process of MoS_2 restacked, polymers can be

[a]*School of Chemical Engineering, Hefei University of Technology, Hefei 23009, China. E-mail: jinwang@hfut.edu.cn; Fax: +86-551-62905660; Tel: +86-551-62905660*

[b]*Department of Electronics and Electrical Engineering, University of Glasgow, G12 8QQ, UK*

[c]*School of Materials Science and Engineering, Hefei University of Technology, Hefei 23009, China*

inserted into the layered host MoS_2 in the following two ways: (1) direct insertion approach, where the polymer are first dispersed in solvent and then inserted into the MoS_2 layered structure; (2) *in situ* intercalation/polymerization approach, where the intercalated monomer was inserted first, followed the monomer polymerized in the present of MoS_2. As for the former, polyaniline (PANI) and its intercalation compounds PANI/MoS_2 have been prepared by mixing a solution of PANI and a suspension of single-layer MoS_2.[22,23] However, the effect of mixing is dependant on the solubility of the conjugated polymer. For most conjugated polymers, poor solubility limits their application in composites. *In situ* intercalation/polymerization are the facile approach for the fabrication of conjugated polymer/MoS_2 composites. The composites of MoS_2 and conjugated polymers such as polypyrrole, polythiophene and its derivates have been prepared by this method.[24–26] The study on PEDOT/MoS_2 composites used for capacitor has not been reported.

The purpose of this work is to enhance the capacitance properties of PEDOT electrode materials *via* introduction of 2D layer MoS_2. PEDOT/MoS_2 intercalated composites were synthesized *via in situ* polymerization in a single layer suspension of MoS_2 with APS as an oxidizing agent. The structure, thermal stability and capacitance performance were examined and the relationship between structure and properties are discussed. The well-defined intercalated structures of PEDOT/MoS_2 composites exhibit improved thermal stabilities and capacitance properties. It can be deduced that a synergistic effect occurs between PEDOT and MoS_2 interlayer.

2 Experimental

2.1 Materials

EDOT monomer (99%), *N*-butyllithium (1.6 M solution in hexane) was obtained from Aladdin industrial Inc. MoS_2 (99%) is from Hefei Kehua Fine Chemical Industry Research Institute. APS, methanol and acetone are from Sinopharm Chemical Reagent Co., Ltd.

2.2 Synthesis of PEDOT/MoS_2 nanocomposites

The suspension of single layer MoS_2 was prepared based on the literature.[27] Commercial raw 2H-MoS_2 was soaked in 1.5 equivalents butyllithium and kept in a nitrogen atmosphere for 3 days. The Li_xMoS_2 product was then exfoliated in water (~100 mL) through a redox reaction. 0.8 mL EDOT was added into a three-necked flask with the different number of single layer MoS_2 suspension (10, 20, 30 mL). This solution was stirred until a homogeneous distribution was obtained. 3.42 g of APS (EDOT–APS molar ratio is 1 : 2) was dissolved into deionized water and added dropwise to the flask followed by mechanical stirring for 72 h at the room temperature. The reaction product was washed using a methanol–acetone mixture (methanol–acetone volume ratio is 2 : 1) followed by distilled water and then put into a vacuum drying oven for desiccation (24 h at 60 °C). The PEDOT/MoS_2 intercalated composites with 14 wt%, 30 wt% and 45 wt% contents of MoS_2 were named PEDOT/MoS_2-14, PEDOT/MoS_2-30, PEDOT/MoS_2-45, respectively. PEDOT without acid doping was also synthesized as above for comparison.

2.3 Characterization

X-ray diffraction (XRD) data were recorded using a Rigaku D/Max-2550 diffractometer with Cu-Kα radiation (λ = 1.5418 Å). The morphology of MoS_2 and PEDOT/MoS_2 nanocomposites was examined using a field emission scanning electron microscope (FE-SEM, SU8020, Hitachi, Japan), operated at an acceleration voltage of 5 kV and equipped with an energy-dispersive X-ray (EDX) spectrometer and a field emission transmission electron microscope (FE-TEM, JEM-2100F, JEOL, Japan, operated at an accelerating voltage of 200 kV). The surface chemical properties of PEDOT/MoS_2 nanocomposites were investigated using EDX spectrometer. The thermal stabilities of all PEDOT/MoS_2 samples were characterized using a TG 209 F3 (Netzsch, Germany) with a heating rate of 10 °C min^{-1} under N_2 atmosphere. Electrical conductivity at room temperature was determined using a conventional four-probe method on pressed pellets, formed under a pressure of 20 MPa with a diameter of 10 mm. Cyclic voltammetry (CV), constant current charge–discharge tests and electrochemical impedance spectroscopy (EIS) experiments were conducted using a CHI660B electrochemical workstation with a three-electrode system. The working electrode was prepared by mixing the PEDOT/MoS_2 powder, carbon black and polyvinylidene fluoride (PVDF) binder (85 : 10 : 5 by weight). The mixture (~0.007 g) was pressed onto the steel mesh (~30 mm^2), and dried under vacuum for 3 h at 60 °C. The thickness of the working electrode is about 0.3 mm. We can think these values are constant. Blank platinum was used as the counter electrode. Ag/AgCl was used as the reference electrode. Experiments were carried out at ambient temperature using 1 M H_2SO_4 aqueous solution as an electrolyte.

3 Results and discussion

3.1 Structure and morphology

The structures of PEDOT, restacked MoS_2 and PEDOT/MoS_2 composites were confirmed by FT-IR spectra. As shown in Fig. 1, the presence of peaks at 1382 and 1350 cm^{-1} (C–C and C=C stretching vibrations of thiophene ring), 1204 and 1095 cm^{-1}

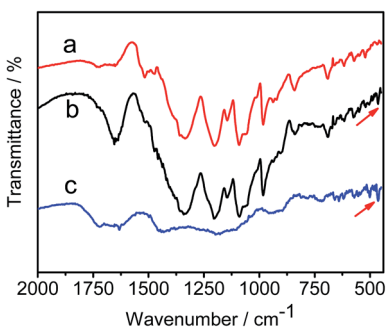

Fig. 1 FT-IR spectra of PEDOT (a), PEDOT/MoS_2 composites (b) and restacked MoS_2 (c).

(C–O–C stretching vibrations in ethylene oxide unit), 984 and 694 cm^{-1} (C–S stretching vibrations in thiophene ring) prove the formation of PEDOT. The peak at about 465 cm^{-1} in restacked MoS_2 is assigned to Mo–S stretching mode of vibration. In comparison with pure PEDOT, the presence of peak at about 465 cm^{-1} in PEDOT/MoS_2 composites proves the existence of MoS_2. The intercalation of PEDOT into the MoS_2 host layers is demonstrated by powder X-ray diffraction. Fig. 2a provides the XRD pattern of the dry restacked MoS_2. This presents an obvious (002) diffraction peak, indicating that the MoS_2 layer is still regularly restacked along the *c*-axis. The restacked MoS_2 shows broadened peaks and a shortened (002) diffraction peak, suggesting that the mean crystallite size of the restacked MoS_2 is much smaller than that of raw bulk 2H-MoS_2.[28] The typical XRD patterns of PEDOT/MoS_2 composites are shown in Fig. 2b. The (001) diffraction peak is observed with shifts to lower angles that indicates an increase in interlayer spacing. The middle strong (001) peak at 6.54° corresponds to $d = 13.79$ Å. Compared with bulk MoS_2, the interlayer spacing of MoS_2 in the intercalation composites was expanded by approximately 7.64 Å due to the intercalation of PEDOT. The strong *c*-axis peaks at $2\theta = 14.3°$ (Fig. 2b) also reveals that partial MoS_2 is still regularly restacked along the *c*-axis without sandwiching PEDOT, and partially intercalated PEDOT/MoS_2 composites are obtained in our experiment. The data from the PEDOT/MoS_2 composites also shows another two broad peaks at *ca.* $2\theta = 18°$ and 26° which are different from those of MoS_2 and should attributed to the diffraction patterns of PEDOT,[29] indicating the periodicity parallel and perpendicular characteristics of the polymer chain. Charge storage in MoS_2 can occur *via* intersheet or intrasheet double-layer charge storage modes,[21] and the well-ordered PEDOT/MoS_2 intercalation composites offer the potential of being good electrode materials.

The morphology and the chemical surface characteristics of MoS_2 and PEDOT/MoS_2 composites were characterized by TEM, SEM and EDX. The TEM image of as-prepared exfoliated MoS_2 shows thin layered particles with a typical size of 350 nm long and 200 nm wide (Fig. 3a). The 2D lamellar MoS_2 with higher specific surface area of MoS_2 is favorable for double layer capacitive properties in comparison with bulk MoS_2. These MoS_2 structures have exhibited typical single-crystal features, as revealed by the SAED pattern (inset in Fig. 3c). The HRTEM

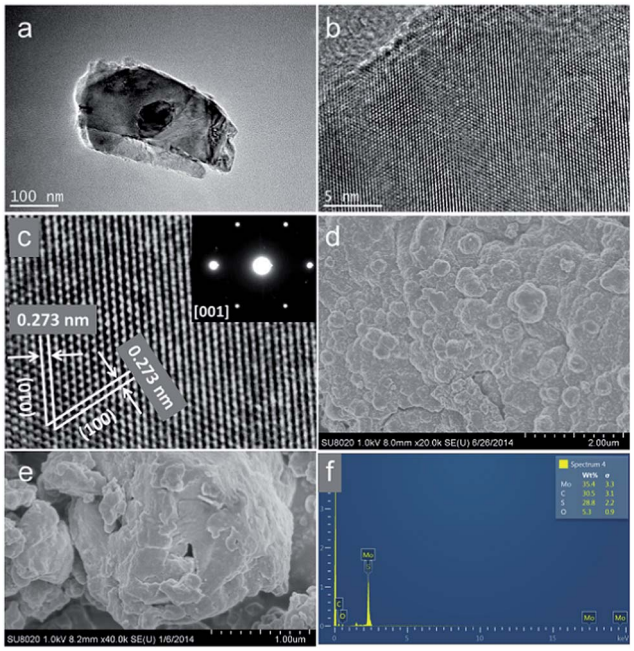

Fig. 3 TEM and HR-TEM images of Li-intercalated MoS_2 (a–c), SEM of PEDOT/MoS_2 (d and e), EDX pattern of PEDOT/MoS_2 (f).

image does show lattice fringes corresponding to MoS_2 (Fig. 3b), two kinds of lattice spacing of 0.273 nm can be observed in the magnified HRTEM image, corresponding to the (100) and (101) planes of standard MoS_2, respectively (Fig. 3c). The combinations of SEM and EDX methodologies not only help to observe PEDOT/MoS_2, they also provide information on the two-dimensional, physico-chemical nature of the composites. Scanning electron micrographs of PEDOT/MoS_2 composites are presented in Fig. 3d and e and EDX spectrograms are shown in Fig. 3f. The morphology of the conjugated polymer strongly depends upon the nature of the anionic oxidizing agents used and preparation methods. As shown in Fig. 3d, PEDOT/MoS_2 composites took on a uniformed state with plate like structure, which is different from the nanoribbon like structure of PEDOT/MoS_2 composites produced using $FeCl_3$ as an oxidizing agent.[26] The existence of Mo, S, C and O are evidenced from EDX analysis performed on the surface of the composites (Fig. 3f), suggesting that MoS_2 and PEDOT exist in the composites.

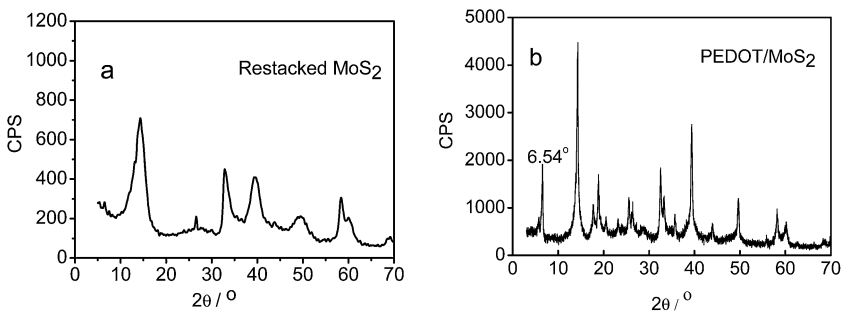

Fig. 2 XRD patterns of restacked MoS_2 (a) and PEDOT/MoS_2 composites (b).

Furthermore, the elemental composition of PEDOT/MoS_2 can calculated by EDX measurements, its chemical ratios of Mo, S, C and O are 35.4 wt%, 28.8 wt%, 30.5 wt% and 5.3 wt%, respectively, which is in general agreement with the product expected from the experiment, showing the composites are uniform.

3.2 Thermal analysis

The thermal analysis of PEDOT and PEDOT/MoS_2 nanocomposites in N_2 atmosphere was obtained using TGA experiments as shown in Fig. 4. All the samples exhibited slight weigh loss in the range of 100–150 °C, which can ascribed to the loss of water. The mass loss which occurs between 250 °C and 400 °C could be attributed to the combustion and departure of the organic polymer components. The maximum weight loss velocity temperature of pure PEDOT and PEDOT/MoS_2 nanocomposites are seen at 313 °C, 323 °C, 349 °C and 365 °C, respectively. It is clear that the thermal stability of PEDOT/MoS_2 intercalated composites were better than that of PEDOT, and the thermal stability of PEDOT/MoS_2 increased with increasing content of MoS_2. 2D layered nanomaterials can improve the properties of polymers, including strength, modulus, thermal stability and gas barrier effects.[30] MoS_2 used as 2D layered nanofillers in PEDOT/MoS_2 composites increase the thermal stability of the PEDOT matrix due a physical barrier effect which retards the diffusion of degradation products, gases and heat. The mass loss is followed by a slight continuous weight loss up to 600 °C, which can be attributed to the complete departure of residual polymer components. There is still 31% weight remaining in pure PEDOT when the temperate reaches 800 °C. This should be attributed to the carbonization of the conjugate ring structure of PEDOT at high temperatures. The remaining weight of PEDOT/MoS_2 composites are around 41%, 54% and 62% at 800 °C, respectively. The weight percentage of MoS_2 in PEDOT/MoS_2 intercalation composites can also be determined by TGA. The weight percentage of MoS_2 can be calculated in the following way. After heated to 800 °C, MoS_2 (weight percentage = x) and the residual of PEDOT ($0.31(1-x)$) remains. So we have $x + 0.31(1-x) = 0.41$, 0.54, and 0.62. The corresponding weight percentages of MoS_2 are 14%, 30% and 45%, respectively.

3.3 Electrical conductivity

Room temperature electrical conductivities were measured on pellets pressed from powders. The conductivity values of restacked MoS_2, pure PEDOT and PEDOT/MoS_2 nanocomposites are summarized in Table 1. The measured conductivity values of restacked MoS_2 and PEDOT were 1.37×10^{-2} S cm^{-1} and 2.43×10^{-2} S cm^{-1}, respectively. However, the measured conductivity values of PEDOT/MoS_2 nanocomposites without any acid doping are an order of magnitude higher than that of each component, *i.e.*, restacked MoS_2 and pure PEDOT. These values increased with increasing amount of MoS_2. The electrical conductivity values of PEDOT/MoS_2-14, PEDOT/MoS_2-30, and PEDOT/MoS_2-45 are 5.56×10^{-1} S cm^{-1}, 7.53×10^{-1} S cm^{-1} and 9.10×10^{-1} S cm^{-1}, respectively. The increase of electrical conductivity in intercalated composites is explained by an interaction between conductive PEDOT and MoS_2 layers. The conducting macromolecules of PEDOT with conjugated π-bonds intercalated into the host interlayer of MoS_2 are arranged in a layered arrangement according the XRD analysis as above. This architecture is advantageous for transportation of electrons between the organic and inorganic components. Moreover, intercalation of MoS_2 with lithium results in a structural transformation from trigonal prismatic to octahedral metal coordination and a change in properties from semiconducting to metallic.[31] Increasing the contents of metallic restacked MoS_2 in PEDOT/MoS_2 nanocomposites can improve the conductivity property.

In comparison with $FeCl_3$ as oxidizing agent,[26] PEDOT/MoS_2 produced using APS as oxidizing agent in this work showed higher conductivity. The electrical conductivity of composites is related to the particle size and shape.[32] Higher surface area for electron transfer is usually favorable for increasing electron mobility, and the smaller particle size provides a higher surface area for electron transfer. The particle size and shape of synthesized PEDOT depends on the oxidant type, PEDOT nanoparticles using APS as the oxidizing agent showed a smaller particle size and higher electrical conductivity than $FeCl_3$. The conductivity of the conjugated polymer is also related to the length of their conjugated chain. The addition of inorganic compounds may decrease the degree of conjugated π bonds in the polymer when using an improper synthesis method.[26,33] APS using as the oxidizing agent can provides a better stability polymerization system in comparison to using $FeCl_3$ as an oxidizing agent. The progressive conductivity of PEDOT/MoS_2 intercalation composites reported here indicates that the preparation method is a facile approach for organic/inorganic composites.

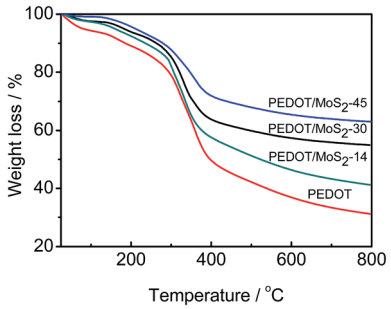

Fig. 4 TGA curves of PEDOT and PEDOT/MoS_2 composites.

3.4 Electrochemical characteristics

The electrochemical behavior of the samples when used as active electrode materials was investigated using CV, EIS and constant current charge–discharge tests in 1.0 M H_2SO_4 aqueous solution. Fig. 5 illustrates the CV performance of pure PEDOT and PEDOT/MoS_2 intercalation composites with different MoS_2 contents at a scan rate of 50 mV s^{-1} in the potential window range of −0.2–0.8 V. These data are normalized to the geometric area of the electrode surface. The voltammograms reveal high electrochemical reversibilities of PEDOT and PEDOT/MoS_2 intercalation composites at this

Table 1 The data of electrical conductivities

Sample	Restacked MoS_2	PEDOT	PEDOT/MoS_2-14	PEDOT/MoS_2-30	PEDOT/MoS_2-45
Conductivity (S cm^{-1})	1.37×10^{-2}	2.43×10^{-2}	5.56×10^{-1}	7.53×10^{-1}	9.10×10^{-1}

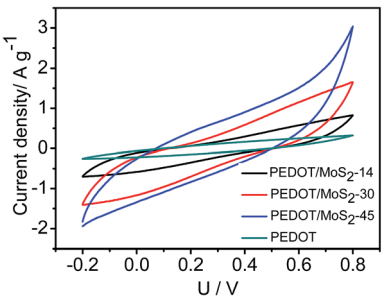

Fig. 5 CV curves of pure PEDOT and PEDOT/MoS_2 composites at scan rate of 50 mV s^{-1}.

potential range and sweep rate. In comparison to pure PEDOT, the CV curves PEDOT/MoS_2 intercalation composites show a deviation from the rectangular shape, whereby the CV profile resembles an 'S'-shape, which suggesting the coexistence of charge storage mechanisms with double layer charge storage and pseudocapacitive faradic charging. The curves show no obvious peaks, indicating that the capacitor assembled using a PEDOT/MoS_2 nanocomposite electrode has fast charge and discharge properties.[34] By comparison, the area of the CV curve for the PEDOT/MoS_2 nanocomposite is larger than those of the pure PEDOT electrode, indicating higher specific capacitance and the synergistic effect of PEDOT and MoS_2. In this case the charge carrier within the electrodes could be more effective and rapid due to the interaction between PEDOT and MoS_2 layers. Furthermore, the CV curve area increases at the same scan rate as the fraction of MoS_2 increases, indicating that the capacitance of PEDOT/MoS_2 nanocomposites increases with the increase in the MoS_2 content. The increase of specific capacitance also suggests that MoS_2 in the composites contributes greatly to the specific capacitance.

Electrochemical impedance measurements were used to study the redox processes of the PEDOT/MoS_2 nanocomposites and to evaluate their ionic and electronic conductivity as well as specific capacitance. The Nyquist plots for PEDOT and PEDOT/MoS_2 nanocomposites with different MoS_2 content are shown in Fig. 6. Impedance was tested in the frequency range from 0.05 kHz to 100 kHz at open-circuit potential. The impedance value was composed of the resistance of the electrode, electrolyte and the contact resistance at the interface active material/current collector. There is great similarity in the Nyquist plots for all of these materials. At high frequency, the plots of PEDOT and PEDOT/MoS_2 intercalation composites all show favourable semicircles which is indicative of the charge transfer phenomena of a faradic redox process. The diameter of the semicircle corresponded to interface charge transfer resistance (R_{ct}). The R_{ct} of PEDOT/MoS_2 is smaller than that of PEDOT, showing PEDOT/MoS_2 composites have the faster charge transfer rates. Meanwhile, the R_{ct} of PEDOT/MoS_2 composites decreased with increasing fraction of MoS_2. This indicates that the addition of MoS_2 reduces charge transfer resistance and improves the conductivity of the electrode materials. At low frequency, the line is almost vertical to the real axis in the imaginary part of the impedance demonstrating an ideal capacitive behavior for PEDOT/MoS_2 nanocomposites. This ideal capacitive behavior is attributed to the faradic pseudocapacitance of the composite electrodes.[35] This conclusion agrees with the capacitance properties above.

3.5 Charge–discharge cycling performance

The galvanostatic charge–discharge curves of PEDOT and PEDOT/MoS_2 are displayed in Fig. 7a. It can be observed that all the charge–discharge curves of PEDOT and PEDOT/MoS_2 took on the shapes that closed to a triangle, and show distinct characteristics of reversible charge–discharge. Particularly, PEDOT/MoS_2 composites have longer charge–discharge times than PEDOT as can be ascribed to their high capacitance performances. The specific capacitance can be evaluated using the following equation:[36]

$$C_g = \frac{I\Delta t}{\Delta V \times m}, \quad (1)$$

where C_g (F g^{-1}) is the specific capacitance of the electrode, I (A) is the discharge current, Δt (s) is the discharge time, ΔV (V) is the potential window and m (g) is the mass of active materials loaded in working electrode. According to the equation, the specific capacitance of PEDOT can be calculated as 109 F g^{-1}. The discharge time of PEDOT/MoS_2 composites increased with increasing MoS_2 content. The specific capacitances of PEDOT/MoS_2-14, PEDOT/MoS_2-30 and PEDOT/MoS_2-45 are 208 F g^{-1}, 354 F g^{-1} and 405 F g^{-1}, respectively. The specific capacitance of the PEDOT/MoS_2-45 sample reached four times that of pure PEDOT. This gives clear proof that a

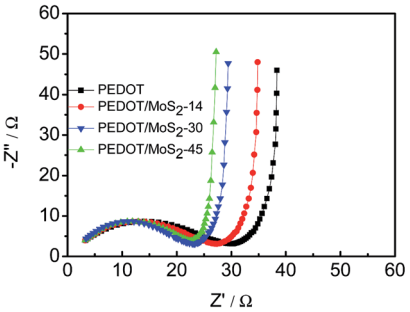

Fig. 6 Nyquist impedance spectra of pure PEDOT and PEDOT/MoS_2 composites.

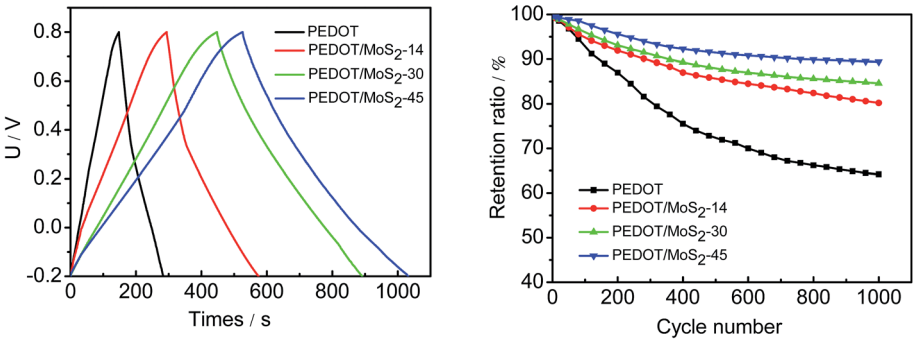

Fig. 7 Galvanostatic charge–discharge curves (a) and cycle stability (b) of electrodes with pure PEDOT and PEDOT/MoS_2 at current density of 0.8 A g^{-1}.

synergistic effect of PEDOT and MoS_2 allows a higher capacitance for the composite electrode which derived from both charge-storage mechanisms. Huang *et al.*[37] and Ma *et al.*[38] has reported the composites of PANI/MoS_2 and PPy/MoS_2 respectively, in which the preparation method of conducted polymer/MoS_2 composites is mainly through chemical synthesis from Mo precursors such as sodium molybdate ($Na_2MoO_4 \cdot H_2O$). PANI/MoS_2 composites exhibit a specific capacitance of 575 F g^{-1} at a current density of 1 A g^{-1} in a three-electrode system, which is about two times than that of pure PANI. The composites of PPy and MoS_2 afforded a high specific capacitance of 553.7 F g^{-1} at a current density of 1 A g^{-1} in a typical three-electrode test, which is also about two times than that of pure PPy. The specific capacitance of these composites all higher than each of the composition, and shows the synergistic effect in conducted polymer/MoS_2 composites. For comparison, the preparation of PEDOT/MoS_2 nanocomposites in this work shows a more effective improvement method in supercapacitance performance.

The cycling stability of PEDOT and PEDOT/MoS_2 nanocomposite electrodes was measured by charge–discharge cycling at a current density of 0.8 A g^{-1}. As shown in Fig. 7b, the specific capacitance of PEDOT is only 64% after 1000 charge–discharge cycles, while the PEDOT/MoS_2 nanocomposite electrodes displayed greater cycle stability, with this stability increasing with increasing fraction of MoS_2. The specific capacitance of the PEDOT/MoS_2-45 sample decreased only 5% after 200 cycles, holding steady at 90% from 300 cycles to 1000 cycles. This demonstrates that PEDOT/MoS_2-45 has good long-term cycle stability. These studies suggest that the composite electrodes have fast charge exchange, leading to good cyclic power storage ability. The excellent cycling stability can be explained by the following two reasons: (1) the higher specific surface area of MoS_2 is favorable to the rapid diffusion of ions by providing a low-resistance pathway and (2) the intercalation of conjugated polymer into the MoS_2 interlayer facilitates electron transport during the charging and discharging processes because of its high conductivity. This result is also in agreement with the thermal stability analysis above, *i.e.*, the better thermal stability of PEDOT/MoS_2 brings smaller volume change during the charge–discharge processes.

4 Conclusions

A facile synthesis method of PEDOT/MoS_2 nanocomposites has been developed *via in situ* polymerization in the presence of ammonium persulfate. The well-defined intercalated structure of PEDOT/MoS_2 nanocomposites is beneficial to their conductivity, thermal stability and capacitance. The conductivity, thermal stability and the specific capacitances of the PEDOT/MoS_2 nanocomposites were enhanced by increasing the amount of MoS_2, exhibiting a good synergetic effect between an inorganic layered compound and organic polymer. When the content of MoS_2 was 45% in weight, the specific capacitance achieved was 405 F g^{-1}, about 4 times larger than that of a PEDOT electrode. The PEDOT/MoS_2 nanocomposite also retained a capacity of around 90% after 1000 cycles. This work offers a strategy for preparing supercapacitors with high performance and good stability.

Acknowledgements

This work was financially supported by National Natural Science Foundation of China (Grant no. 61076040), Anhui Provincial Natural Science Foundation (Grant no. 1208085MB23).

References

1 A. Burke, *J. Power Sources*, 2000, **91**(1), 37.
2 S. L. Candelaria, Y. Y. Shao, W. Zhou, X. L. Li, J. Xiao, J. G. Zhang, Y. Wang, J. Liu, J. H. Li and G. Z. Cao, *Nano Energy*, 2012, **1**, 195.
3 S. Chen, J. W. Zhu, X. D. Wu, Q. F. Han and X. Wang, *ACS Nano*, 2010, **4**, 2822.
4 D. Choi, G. E. Bloragren and P. N. Kumm, *Adv. Mater.*, 2006, **18**, 1178.
5 K. Firoz Babu, S. P. Siva Subramanian and M. Anbu Kulandainathan, *Carbohydr. Polym.*, 2013, **94**(1), 487.
6 S. R. P. Gnanakan, M. Rajasekhar and A. Subramania, *Int. J. Electrochem. Sci.*, 2009, **4**, 1289.
7 Q. Liu, O. Nayfeh, M. H. Nayfeh and S. T. Yau, *Nano Energy*, 2013, **2**, 133.

8 J. F. Mike and J. L. Lutkenhaus, *J. Polym. Sci., Part B: Polym. Phys.*, 2013, **51**(7), 468.
9 T. Brezesinski, J. Wang, S. H. Tolbert and B. Dunn, *Nat. Mater.*, 2010, **9**, 146.
10 U. K. Sen and S. Mitra, *ACS Appl. Mater. Interfaces*, 2013, **5**(4), 1240.
11 S. Y. Liew, D. A. Walsh and W. Thielemans, *RSC Adv.*, 2013, **3**, 9158.
12 M. Ghaffari, S. Kosolwattana, Y. Zhou, N. Lachman, M. Lin, D. Bhattacharya, K. K. Gleason, B. L. Wardle and Q. M. Zhang, *Electrochim. Acta*, 2013, **112**, 522.
13 P. Sharma and T. S. Bhatti, *Energy Convers. Manage.*, 2010, **1**, 2901.
14 T. Lindfors, A. Österholm, J. Kauppila and M. Pesonen, *Electrochim. Acta*, 2013, **110**, 428.
15 K. S. Ryu, Y. G. Lee, Y. S. Hong, Y. J. Park, X. L. Wu, K. M. Kim, M. G. Kang, N. G. Park and S. H. Chang, *Electrochim. Acta*, 2004, **50**, 843.
16 R. Ranjusha, K. M. Sajesh, S. Roshny, V. Lakshmi, P. Anjali, T. S. Sonia, A. S. Nair, K. R. V. Subramanian, S. V. Nair, K. P. Chennazhi and A. Balakrishnan, *Microporous Mesoporous Mater.*, 2014, **186**, 30.
17 H. Zhou, W. Yao, G. Li, J. Wang and Y. Lu, *Carbon*, 2013, **59**, 495.
18 Y. T. Weng and N. L. Wu, *J. Power Sources*, 2013, **238**, 69.
19 F. Schedin, A. K. Geim, S. V. Morozov, E. W. Hill, P. Blake, M. I. Katsnelson and K. S. ovoselov, *Nat. Mater.*, 2007, **6**, 652.
20 C. C. Hu, K. H. Chang, M. C. Lin and Y. T. Wu, *Nano Lett.*, 2006, **6**, 2690.
21 J. M. Soon and K. P. Loh, *Electrochem. Solid-State Lett.*, 2007, **10**(11), 250.
22 M. G. Kanatzidis, R. Bissessur, D. C. DeGroot, J. L. Schindler and C. R. Kannewurf, *Chem. Mater.*, 1993, **5**, 595.
23 R. Bissessur and W. White, *Mater. Chem. Phys.*, 2006, **99**, 214.
24 L. Wang, J. Schindler, J. A. Thomas, C. R. Kannewurf and M. G. Kanatzidis, *Chem. Mater.*, 1995, **7**, 1753.
25 B. Z. Lin, C. Ding, B. H. Xu, Z. J. Chen and Y. L. Chen, *Mater. Res. Bull.*, 2009, **44**, 719.
26 A. V. Murugan, M. Quintin, M. H. Delville, G. Campet, C. S. Gopinath and K. Vijayamohanan, *J. Power Sources*, 2006, **156**, 615.
27 M. A. Gee, R. F. Frindt, P. Joensen and S. R. Morrison, *Mater. Res. Bull.*, 1986, **21**, 543.
28 G. Du, Z. Guo, S. Wang, R. Zeng, Z. Chen and H. Liu, *Chem. Commun.*, 2010, **46**, 1106.
29 N. Paradee and A. Sirivat, *Polym. Int.*, 2014, **63**, 106.
30 K. Q. Zhou, Q. J. Zhang, J. J. Liu, B. Wang, S. H. Jiang, Y. Q. Shi, Y. Hu and Z. Gui, *RSC Adv.*, 2014, **4**, 13205.
31 J. Heising and M. G. Kanatzidis, *J. Am. Chem. Soc.*, 1999, **121**, 11720.
32 N. Paradee and A. T. Sirivat, *Polym. Int.*, 2014, **63**, 106.
33 X. X. Bai, X. J. Hu, S. Y. Zhou, J. Yan, C. H. Sun, P. Chen and L. F. Li, *Electrochim. Acta*, 2013, **106**, 219.
34 D. Wei, S. J. Wakeham, T. W. Ng, M. J. Thwaites, H. Brown and P. Beecher, *Electrochem. Commun.*, 2009, **11**, 2285.
35 R. Kötz and M. Carlen, *Electrochim. Acta*, 2000, **45**, 2483.
36 Y. Q. Han, M. X. Shen, J. J. Zhu, Y. Wu and X. G. Zhang, *Polym. Compos.*, 2013, **34**, 989.
37 K. J. Huang, L. Wang, Y. J. Liu, H. B. Wang, Y. M. Liu and L. L. Wang, *Electrochim. Acta*, 2013, **109**, 587.
38 G. F. Ma, H. Peng, J. J. Mu, H. H. Huang, X. Z. Zhou and Z. Q. Lei, *J. Power Sources*, 2013, **229**, 72.